Ionic and conformational mobility in poly(vinylidene fluoride)/ionic liquid blends: Dielectric and electrical conductivity behavior

D. M. Correia[1], R. Sabater i Serra[2,3], J.A Gómez Tejedor[2], V. de Zea Bermudez[1], A. Andrio Balado[4], J..M Meseguer Dueñas[2,3], J. L. Gomez Ribelles[2,3], S. Lanceros-Méndez[5,6], C. M. Costa[7*]

[1]Department of Chemistry and CQ-VR, University of Trás-os-Montes e Alto Douro, 5000-801 Vila Real, Portugal
[2]Centre for Biomaterials and Tissue Engineering, CBIT, Universitat Politècnica de València, 46022 Valencia, Spain
[3]Biomedical Research Networking Center on Bioengineering, Biomaterials and Nanomedicine (CIBER-BBN), Valencia, Spain
[4]Departament de Física, Universitat Jaume I, 12071 Castelló, Spain
[5]BCMaterials, Parque Científico y Tecnológico de Bizkaia, 48160-Derio, Spain
[6]IKERBASQUE, Basque Foundation for Science, 48013, Bilbao, Spain
[7]Centro de Física, Universidade do Minho, 4710-057 Braga, Portugal

Abstract:

The glass transition dynamics and the charge transport for blends composed of poly(vinylidene fluoride (PVDF) and the ionic liquid (IL) 1-ethyl-3-methylimidazolium bis(trifluoromethylsulfonyl) imide, [Emim][TFSI] with different IL content (0, 10, 25 and 40 % wt.) prepared by solvent casting at 210 °C have been investigated by differential scanning calorimetry (DSC), dynamic-mechanical analysis (DMA) and broadband dielectric relaxation spectroscopy (BDS) in wide frequency and temperature ranges (0.1 Hz to 1 MHz and -120 to 150 °C, respectively). The inclusion of the IL in the polymer matrix affected the main relaxation process (β-relaxation) of the amorphous phase of the polymer matrix detected with all the techniques employed. The blends were homogeneous regardless of the amount of IL and the glass transition temperature (T_g) shifted to lower temperatures as the IL content was increased. A good agreement between the T_g measured by BDS and DSC was observed for all PVDF/IL samples. The conductivity formalism revealed significant contributions of the IL concentration to the conductivity behavior of the blends in that is described by charge motion and electrode polarization effects. The activation energy of all the PVDF/IL samples, calculated by Dyre model, decreased with IL addition with respect to that of neat PVDF.

Keywords: PVDF; ionic liquid; dielectric response; conductivity; electric modulus

*corresponding author

1. Introduction

In recent years, advances in technology for portable devices, but also for transport applications, such as hybrid electric vehicles (PHEV) and electric vehicles (EV), has led to an increasing demand in the battery sector for improvement of the batteries' safety, energy density and power, and also for the reduction of their cost and weight [1].

The transport sector requires an improvement of the energy density of lithium (Li) ion batteries of 2 to 5 times, while reducing cost and considering environmental (safety) problems [2, 3]. The polymer electrolyte (PE) in the lithium ion battery devices can play an important role to achieve these goals [4].

PEs are a (ionic salts and/or ionic liquids (ILs)) a class of macromolecular systems with a high ionic conductivity ($>10^{-7}$ $S.cm^{-1}$) [5, 6]. Basically, these materials are composed of guest species (ionic salts or ionic liquids (ILs)) dissolved in a host polymeric matrix. Different nanofillers (ceramic, metallic, etc.) can be added mainly to further improve the mechanical and electrochemical properties [7-9].

In this research field, it has been recognized that poly(vinylidene fluoride) (PVDF) is a polymeric matrix of significant interest because of its strong polarity (high dipolar moment) and high dielectric constant with respect to other polymeric materials, which can aid the ionization of ionic salts [10]. In addition, PVDF is known for its electroactive behavior (piezo, pyro and ferroelectric properties) and its good chemical and thermal stability, as well as excellent mechanical properties [11, 12]. The piezoelectric properties of PVDF are particularly attractive for the application in Li ion batteries. It has been shown that in a conventional lithium ion battery, the piezoelectric potential of a PVDF film, created by mechanical stress, acts as a charge pump to drive Li^+ ions to migrate from the cathode to the anode following the reactions of load on the electrodes improving its performance [13, 14].

ILs are one the more propitious compounds for Li ion batteries, since they solve safety problems due of their physicochemical features, including their good chemical and electrochemical stability, non-flammability, negligible vapor pressure and high ionic conductivity [15, 16].

ILs can be classed as aprotic or protic depending on the nature of cation, their structure and properties being largely determined by the choice of the cation and anion [15, 17]. There are thousands of possible ILs available with a wide variety of properties, such as density, vapor pressure, viscosity, conductivity, diffusion, thermal stability, compatibilities and solubility [18, 19].

Various IL, such as 1-vinyl-3-butylimidazolium chloride [Vbim][Cl] [20, 21], 1-vinyl-3-ethylimidazolium tetrafluoroborate ([Veim][BF_4]) [22-24],1-butyl-3-methylimidazolium hexafluorophosphate [Bmim][PF_6] [25], *N*,*N*,*N*-trimethyl-*N*-(2-hydroxyethyl)ammonium bis(trifluoromethylsulfonyl)imide ([$N_{1\,1\,1\,2(OH)}$][TFSI]) and 1-ethyl-3-methylimidazolium ethylsulfate ([Emim][C_2SO_4]) [26] and 1-ethyl-3-methylimidazolium bis(trifluoromethylsulfonyl)imide ([Emim][TFSI]) [27] have been incorporated into the PVDF matrix in order to understand the interaction between the polymer chain and the IL, but also to improve PVDF's electrical, mechanical and thermal properties. In PVDF/IL composites, the ions may be present either as free ions, contact ion pairs or alternatively as diffusion ion pairs in which the IL are good glass-formers.

Understanding the ionic and molecular interactions between the ions (charged species) and the polymeric matrix, the formation of ion pairs, larger ion clusters, the contribution of ions to the electric properties (translation diffusion) and the dynamic glass transition are major issues for improving ionic conductivity in PEs [28, 29]. The ionic transport behavior depends of salt dissociation, salt concentration, dielectric constant of the host polymeric matrix, degree of ion aggregation and segmental mobility of the polymer chains [30].

Broadband dielectric spectroscopy (BDS) is widely used to obtain information about electric properties and molecular dynamics which can be related to the motion of the charged species and of the permanent dipoles in polymers [31, 32]. Thus, for instance, in the case of the poly(1-ethyl-3-vinylimidazolium bis(trifluoromethanesulfonylimide)) polymerized IL, BDS revealed the presence of three relaxation modes including that due to the effect of electrode polarization behavior [33]. The electrode polarization is an phenomenon that occurs in the interface between a metal surface related to the mechanism of charge transport at the interface [34]. In poly(ethylene oxide) (PEO)-based polyurethane ionomers containing mobile Li^+ or Na^+ ions BDS revealed the contributions of free ion concentration and ion mobility to electrode polarization [35].

Recently, the dielectric relaxation and conductivity of PEs composed of a small amount (0.01–10 wt %) of the 1-ethyl-3-methylimidazolium nitrate ([Emim][NO_3]) IL and PVDF were investigated by BDS. The dielectric response was found to be governed by a pronounced low-frequency relaxation which showed typical signatures of electrode polarization, whereas the main dipolar dielectric relaxation, associated with the glass transition, disappeared for IL contents higher than 1 wt %, indicating that the amorphous phase lost its glass-forming properties and underwent structural changes [36]. On the

other hand, DC conductivity and conductivity relaxation in PVDF/[BMIM][PF_6] composites demonstrated that the incorporation of ILs into the matrix accelerated DC conductivity [37].

The goal of the present work is to analyze the miscibility and interaction between an IL and the polymer chains of PVDF through the analysis of the segmental mobility at the glass transition region of the polymer by Differential Scanning Calorimetry (DSC). The dielectric and dynamic-mechanical relaxation spectra were evaluated and the ionic mobility characterized by BDS. The IL used in this work was [Emim][TFSI] as it is a promising IL for battery applications owing to its high ionic conductivity and high thermal stability [38, 39]. PVDF/IL blend films were prepared by solvent casting with high IL content (10-40 wt%).

2. Experimental section

2.1.Materials

PVDF (Solef 6020, MW = 700 kDa), N,N-dimethylformamide (DMF, 99.5 %) and [Emim][TFSI] were acquired from Solvay, Merck and Iolitec, respectively.

2.2.Preparation of the films

PVDF was dissolved in DMF in a 15/85 weight ratio under magnetic stirring at room temperature. After the complete dissolution of the polymer, different contents of [Emim][TFSI] were added to the PVDF solution: 0, 10, 25 and 40 % wt. PVDF/[Emim][TFSI] films (≈ 50 μm thick) were obtained after spreading the solution at room temperature on a glass substrate followed by solvent evaporation at 210 ºC in an air oven. Thus, the blends will be identified henceforth as PVDF/[Emim][TFSI]X, where X is the IL content (0, 10, 25 and 40%).

2.3.Characterization techniques

Differential Scanning Calorimetry (DSC) was carried out with a DSC 8000 of Perkin-Elmer under a flowing nitrogen (N_2) atmosphere between -120 ºC and 200 ºC at a heating rate of 20 ºC/min. The mass of the sample was between 5 and 10 mg.

Dynamic-Mechanical Analysis (DMA) was performed in a PerkinElmer DMA 800 apparatus in tensile mode. The storage modulus and loss tangent were measured as a function of temperature at a frequency of 1 Hz from -90 to 90 ºC at a heating rate of 2 ºC/min. The typical dimension of each sample was 10×4×0.050 mm^3.

Dielectric measurements were carried out in an impedance analyzer Alpha-S in a frequency range from 0.1 Hz to 1 MHz where the temperature control was assured by a Quatro Cryosystem from Novocontrol GmbH. The sample cell with active head dielectric converter was mounted on a cryostat (BDS 1100) and exposed to a heated gas stream evaporated from a liquid N_2 Deward. Circular gold electrodes (10 mm diameter) were deposited onto both sides of each sample, to form a parallel plate capacitor, by sputtering with a Polaron Coater SC502 under an argon atmosphere. The isothermal experiments were performed from −120 to 150 °C (thermal stability: 0.5 °C) in 5 °C steps through the measurement of the capacitance (C) and the loss factor (tan δ), while the complex dielectric permittivity $\varepsilon^* = \varepsilon' - i\varepsilon''$ was determined as a function of frequency.

3. Results and discussion

3.1. Thermal and mechanical analyses

The thermal behavior of the PVDF/[Emim][TFSI] samples was investigated by DSC. The thermograms recorded on heating scans are shown in Figure 1. PVDF/[Emim][TFSI] are blends of two glass-formers. Typically, the PVDF glass transition value reported in the literature is about -40 °C [40] which is similar to that observed for pristine PVDF (Figure 1a).

As shown in the inset of Figure 1a, the thermogram of [Emim][TFSI] exhibits the glass transition in the temperature interval between -100 and -88ºC with a value of glass transition temperature (T_g) of -95 ºC. The exothermic peak around -60 ºC appears immediately after the glass transition and is ascribed to a cold crystallization. The endothermic peak emerging at higher temperatures with a maximum at - 2 ºC corresponds to the melting temperature [41]. In both transitions, the existence of the double peak is due to the existence of various crystalline modifications of [Emim][TFSI] [41].

The thermogram of the PVDF/[Emim][TFSI] 40% blend is that expected for a miscible blend. It shows a broad glass transition with onset in the range of the glass transition of [Emim][TFSI] and ending around -30 ºC as in PVDF (Figure 1a). The broad temperature of the glass transition is due to local fluctuations of the blend composition yielding local T_g fluctuations.

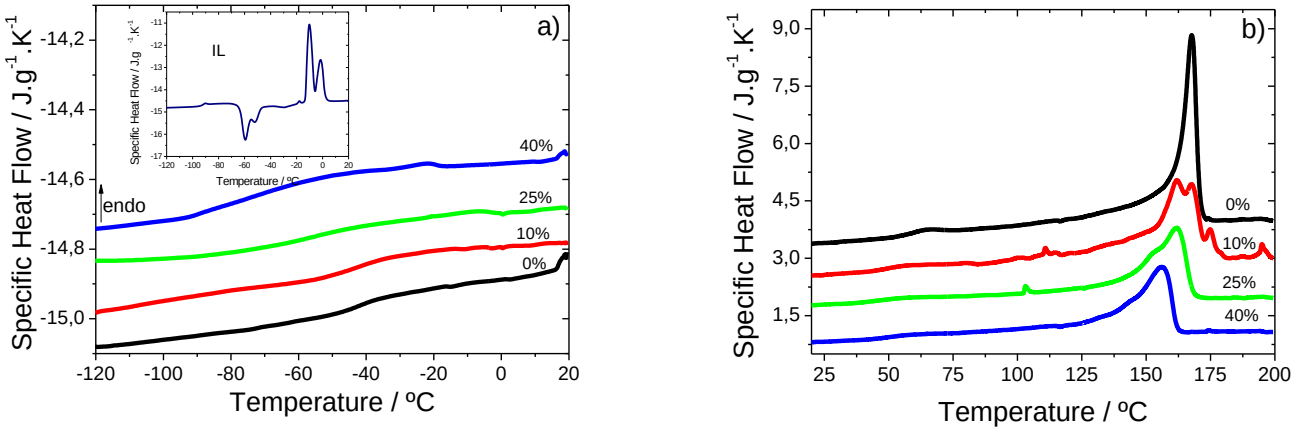

Figure 1 - Specific heat flow per gram vs temperature for all PVDF/[Emim][TFSI] samples between -120 and 20 ºC (a), and between 25 and 200 ºC (b).

For intermediate compositions, the behavior is also similar to that of miscible blends, with the glass transition shifting towards lower temperatures as the [Emim][TFSI] content increases. The T_g values era listed in Table 1. However, it should be noted that the blend PVDF/[Emim][TFSI]10% has a T_g practically equal to that of pure PVDF and this fact will be confirmed below, when analyzing the main mechanical or dielectric relaxation.

In addition it may be inferred from the Figure 1a) that for samples containing 25 and 40% of [Emim][TFSI] the appearance of a small endothermic peak is seen at -25 and 10 ºC, respectively, that can may be correlated with the melting of small amounts of [Emim][TFSI] crystals.

Figure 1b) reproduces the DSC traces of the PVDF/[Emim][TFSI] samples between 25 and 200 ºC showing the effect of the addition of the [Emim][TFSI] on the melting of PVDF. The values of the melting temperature (T_m) and the degree of crystallinity ($\Delta\chi_c$) are collected in Table 1. The $\Delta\chi_c$ value was calculated by the following equation [20]:

$$\Delta\chi_C = \frac{\Delta H_m}{(1 - W_{IL}) \times \Delta H_m^0} \times 100 \quad (1)$$

where ΔH_m is the melting enthalpy of the PVDF/[Emim][TFSI] samples, W_{IL} is the [Emim][TFSI] weight fraction in the PVDF/[Emim][TFSI] samples and ΔH_m^0 is the melting enthalpy of fully crystalline PVDF (103.4 J/g) [42].

Table 1 – Glass transition temperature (T_g), melting temperature (T_m) and degree of crystallinity ($\Delta\chi$) for PVDF/[Emim][TFSI]X samples.

Samples	**T_g / ºC**	**T_m / ºC**	**ΔX / %**
0%	-43	168	50
10%	-45	162	45
25%	-65	162	37.5
40%	-73	156	32.4
[Emim][TFSI]	-95	-------	----------

Table 1 shows that T_m and $\Delta\chi$ decreased with the increase of the [Emim][TFSI] amount. It can be deduced from these results that the IL destabilized the crystalline phase of the PVDF polymer due to the electrostatic interactions established between both components [43].

It has been reported in the literature that in the case of polymer blends with high IL content, there are two competitive effects on the crystallization behavior of the host polymer: on the one hand the promotion of polymer nucleation, but on the other, confinement effects leading to imperfections in the crystalline lamellae [44].

Further insight into miscibility was obtained by means of DMA. The plasticizing effect of [Emim][TFSI] on the main relaxation (β-relaxation) and the broadening of the temperature interval of the relaxation reveals the formation of a homogeneously mixed phase. Figure 2 shows the temperature dependence of the real part of the complex mechanical module E' and tan δ for the PVDF/[Emim][TFSI] samples for a fixed frequency (f =1 Hz).

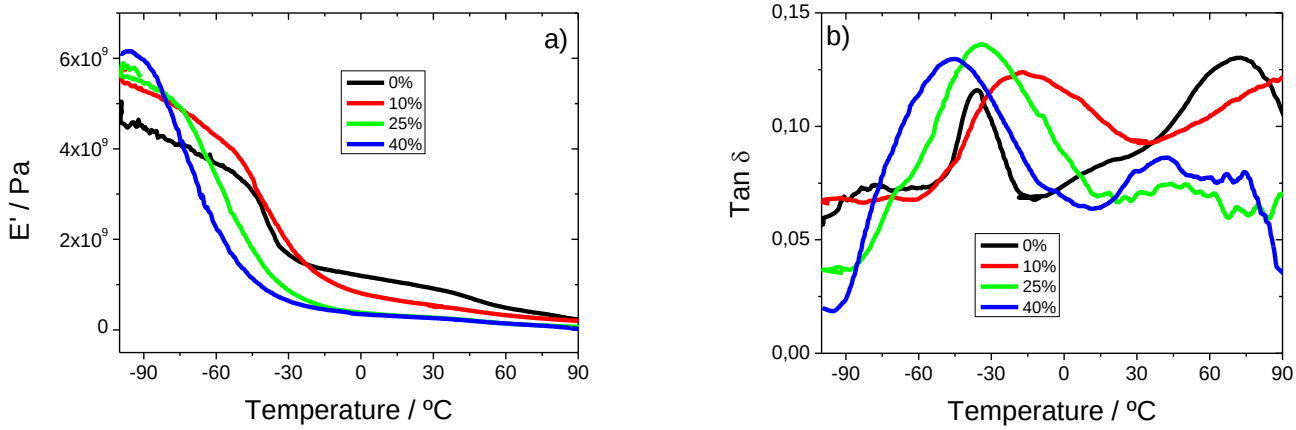

Figure 2 – E' (a) and tan δ (b) vs temperature for the PVDF/[Emim][TFSI] samples.

The main relaxation process of the PVDF polymer, the β-relaxation, related with the glass transition, is a broad relaxation process that can be observed in the tan δ range between -50 and -10 ºC. At higher temperatures (above 60 ºC) the α_c-relaxation appears. The latter relaxation is ascribed to molecular motions within the crystalline fraction of the material [45].

Figure 2a) shows the real part of the complex elastic modulus E' with the two decreasing steps corresponding to the two abovementioned relaxation processes. Figure 2b) shows the tan δ peak from -90 to 30 ºC corresponding to the β-relaxation for all the PVDF/[Emim][TFSI] samples. The strength in the E' decrease as the IL content increases. In both diagrams the important broadening of the temperature interval of the β-relaxation is in perfect agreement with the DSC results. The shift of the relaxation towards lower temperatures, the increase of its strength and the broadening are all indications of the participation of the [Emim][TFSI] molecules in the cooperative conformational

rearrangements of the PVDF chains, and thus the mixing of both components at the molecular scale. Interestingly, the strength of the α_c-relaxation, associated with the movements of the crystallites, rapidly decreases with the increase of IL content, and in fact the step in E' cannot be observed in the traces of Figure 2a, although a small, broad peak in tan δ appears in Figure 2b.

In Figure 2b) in the case of the PVDF/[Emim][TFSI]10% sample the onset of the tan δ peak for β-relaxation is nearly coincident with that of pure PVDF. Nevertheless, since the relaxation is much broader in the blend, the relaxation peak extends towards higher temperatures and the maximum appears at temperatures slightly higher than in pure PVDF. This result is also in agreement with the DSC curves extended (Figure 2b), in which the peak for α_c-relaxation is also observed at temperatures slightly higher than pure PVDF.

3.2.Dielectric analysis

3.2.1. Dielectric and electric modulus formalism

The temperature dependence of the real and imaginary parts of the complex dielectric permittivity for the PVDF/[Emim][TFSI] samples at 1 Hz is shown in Figure 3 a) and 3b), respectively.

For all PVDF/[Emim][TFSI] samples ε' and ε" increase with increasing temperature due basically to different processes: DC conductivity, electrode polarization, Maxwell-Wagner relaxation and charge motion and transport [28]. Moreover, it is verified that both ε' and ε" increase with increasing IL content due to the decoupling and ion transport of the IL, resulting in higher number of carriers in the polymer matrix [26]. In Figure 3b) only for neat PVDF a peak around -40 ºC, related to the β-relaxation, is detected. For the other samples, this peak is not observed due to the overlapping of the conductivity component. Figures 3c) and 3d) show the real and imaginary part of the complex dielectric permittivity, respectively, as a function of frequency for PVDF/[Emim][TFSI] samples at 20 ºC where the effect of the electrode polarization is detected. The large values of ε' and ε" at low frequencies for samples with high IL content are due to the electrode polarization effect caused by the accumulation of ionic charge carriers at the electrode-sample interface [46].

The electric modulus formalism provides a more clear characterization of the dipolar relaxation mechanisms.

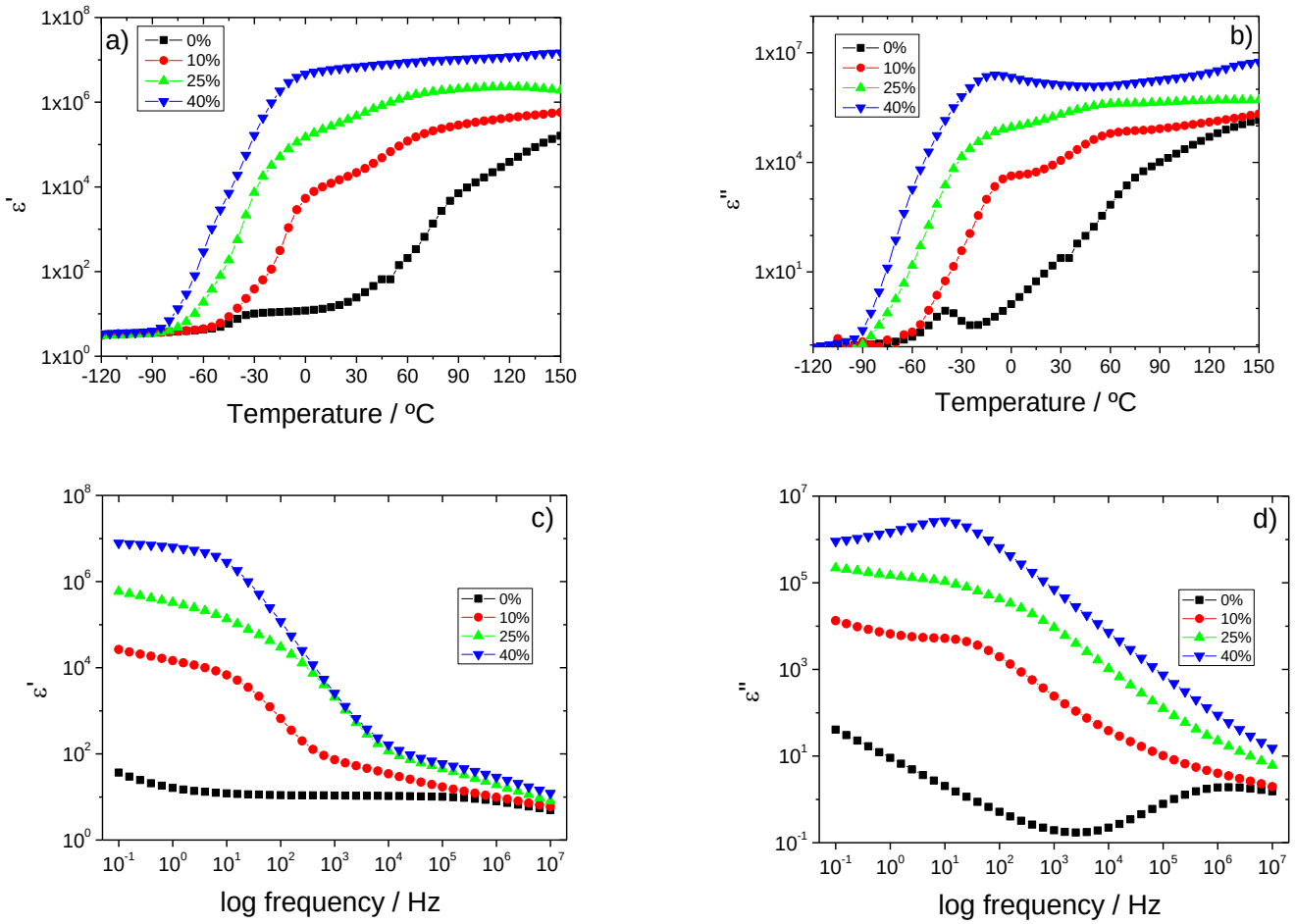

Figure 3 – ε' (a and c) and ε'' (b and d) vs temperature at 1 Hz and frequency for 20 ºC, respectively for all PVDF/IL samples.

The complex electric modulus M^* is defined as the reciprocal of the complex relative permittivity, $\varepsilon^*(\omega)$:

$$M^*(\omega) = 1/\varepsilon^*(\omega) = M'(\omega) + iM''(\omega) = \frac{\varepsilon'(\omega)}{\varepsilon'^2(\omega)+\varepsilon''^2(\omega)} + i\frac{\varepsilon''(\omega)}{\varepsilon'^2(\omega)+\varepsilon''^2(\omega)} \qquad (2)$$

where M′, M′′ are the real and imaginary components of the complex electric modulus, respectively.

Figure 4 shows the imaginary part of the complex modulus for all PVDF/[Emim][TFSI]X samples between -90 and 10 ºC, where the β-relaxation is detected. Another dipolar relaxation, named γ-relaxation, is detected for neat PVDF and for IL=10% at low temperatures below -80 ºC. The latter relaxation is ascribed to local mobility [45]. It can also be observed that the M" spectra are asymmetric when the temperature increases and

skewed towards for higher frequencies for all the doped samples, suggesting fast ionic motion [47].

The relaxation time for each isochronal plot is calculated from the frequency of the maximum of M" using the following equation:

$$\tau = \frac{2\pi}{\omega} \tag{3}$$

where τ is the relaxation time and ω is the frequency.

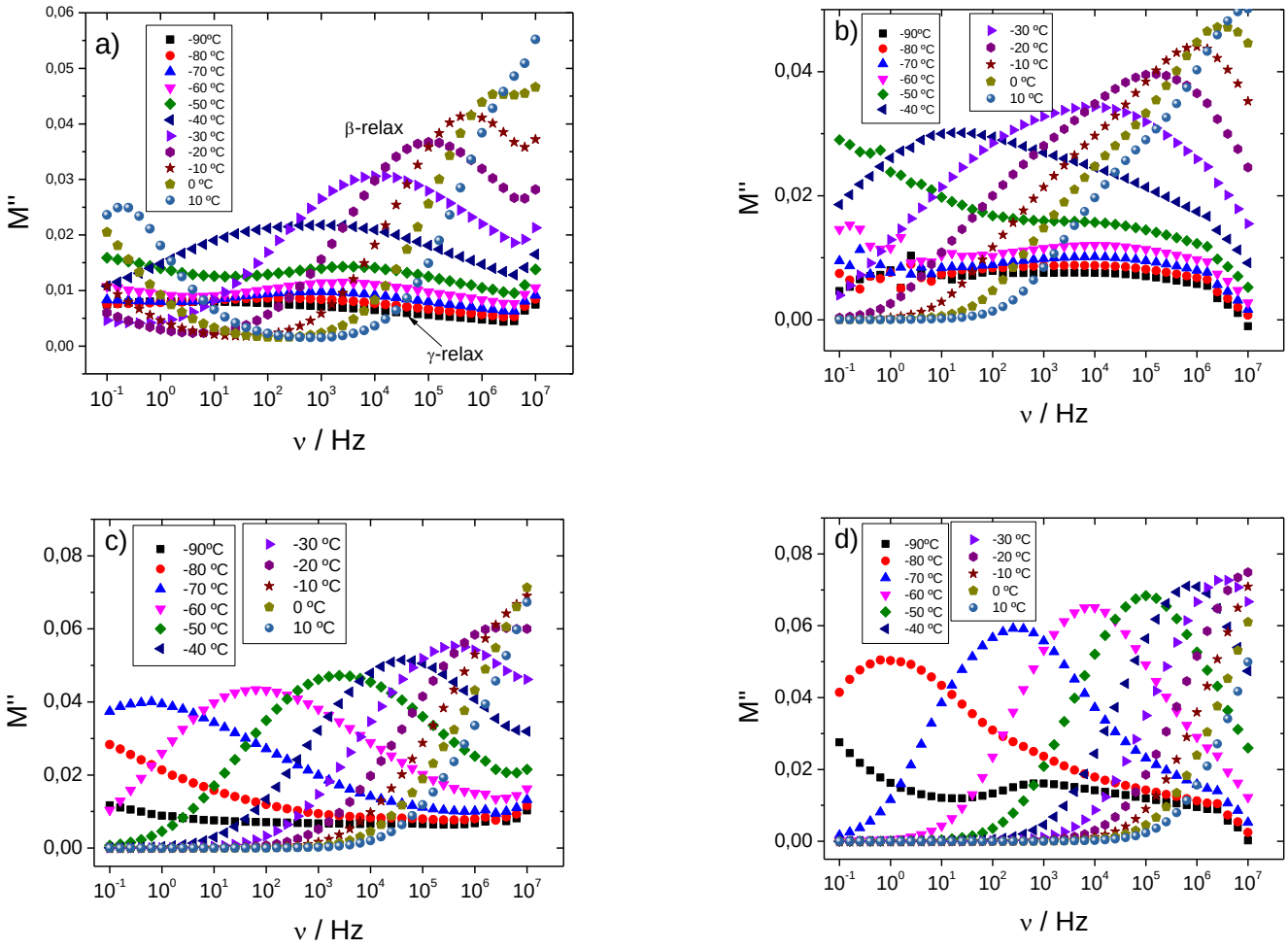

Figure 4 – Isothermal spectra of the imaginary part of the complex modulus for neat PVDF (a), and for PVDF/[Emim][TFSI]10% (b), PVDF/[Emim][TFSI]25% (c) and PVDF/[Emim][TFSI] 40% (d).

The dynamics of the β-relaxation observed for the PVDF/[Emim][TFSI] samples (Figure 4) was analysed in the scope of the Vogel-Fulcher-Tammann (VFTH) formalism [48]:

$$\tau(T) = \tau_0 e^{\frac{B}{T-T_0}} \tag{4}$$

where τ_0 is the relaxation time for infinite temperature, B is a constant and T_0 (Vogel temperature) is the temperature where all the chain motions in equilibrium are frozen (usually 30–70 K below T_g).

The fitting of Eq. (4) to the experimental results and the fitting parameters for β-relaxation are represented in Figure 5 and Table 2, respectively.

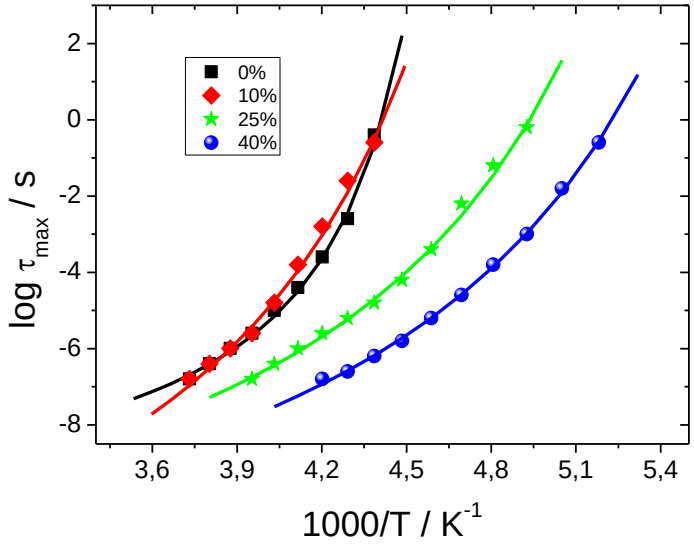

Figure 5 - VFTH fitting for the β-relaxation obtained from M'' (isochronal curves).

If we replace the VFTH expression (Eq. (4)) in the apparent activation energy equation as a function of temperature:

$$E_a(T) = \frac{d \ln \tau}{d \, 1/T} = \frac{R \cdot B}{\left(1 - T_0/T\right)^2} \tag{5}$$

where R is ideal gas constant.

From the VTFH fitting parameters, the fragility parameter [49] is calculated:

$$m(T_g) = \frac{E_a(T_g)}{\ln 10 R \cdot T_g} \tag{6}$$

where *m* is an indication of the steepness of the variation of the material properties (viscosity, relaxation time, …) as T_g is reached. A high *m* value defines a fragile material, whereas a strong material is characterized by small *m* values [50].

We have estimated the dielectric glass transition temperature, Tg-diel, by replacing τ by 100 s in Eq. (4). Table 2 shows all the VFTH fitting parameters and the activation energy of the β-relaxation for the PVDF/[Emim][TFSI] samples.

Table 2 - VFTH fitting parameter and apparent activation energy (τ=100s) obtained for the β-relaxation of the PVDF/[Emim][TFSI] samples.

Samples	Temperature range / ºC	τ_0 (s)	B (K)	T_0 (K)	E_a (KJmol^{-1}) τ=100 s	$T_{g\text{-}diele}$ / ºC	m
PVDF	[-45, -5]	1.46E-10	440.9	2.07E+02	698.2	-50	163.33
10%	[-50, -5]	9.10E-15	1368.3	1.84E+02	405.2	-52	95.73
25%	[-70, -20]	8.47E-13	1105.7	1.63E+02	306.1	-76	81.20
40%	[-80, -35]	3.20E-13	1080.2	1.54E+02	296.8	-87	83.33

The main dielectric relaxation in an amorphous polymer is due to chain segment rearrangements involving a region of the material called cooperative rearranging region, CRR with a characteristic dimension that increases with decreasing temperature, reaching a value of few nanometers at T_g [51-54]. The presence of [Emim][TFSI] inside the CRR mixed with the PVDF chain segments decreased the total energy involved in the rearrangement because individual ions of the IL are more mobile than the chain segments due to chain connectivity. This is why the E_a decreases with increasing IL content in the blend and the curvature of the $\ln\tau$ vs $1/T$ curves of Figure 5 decreases (the material becomes stronger, fragility decreases) while shifting towards lower temperatures when the fraction of [Emim][TFSI] in the blend is higher.

The τ_0 factor for samples with IL amount is of the order > 10^{-13} s, as the typical values for non-cooperative Debye process originated by local orientational fluctuations [55].

A rough estimate of the equivalent frequency of DSC can be obtained within Donth's fluctuation model [56]:

$$f_{eq,DSC} = \frac{q'}{2\pi\alpha\delta T} \quad (7)$$

where q' is the cooling rate, α is a constant on the order of 1, and δT is the mean temperature fluctuation (on the order of 2 ºC). In this work, the $f_{eq,DSC}$ is 0.027 Hz, or a relaxation time of τ_{Tg} = 230 s. The T_g values, determined as the temperature at which the dielectric relaxation time is τ_{Tg}, are listed in Table 2, showing the good agreement between BDS and calorimetric data for all the PVDF/[Emim][TFSI] samples.

3.2.2. Conductivity formalism

To understand the relaxation dynamics of the transport of charge carriers and the electrode polarization, it is appropriate to represent the dependence of frequency and temperature of the complex conductivity, σ *, which can be calculated from the dielectric function by the following equation:

$$\sigma^* = \sigma'(\omega) + i\sigma''(\omega) \quad (8)$$

Thus, the real part of the conductivity is given by:

$$\sigma'(\omega) = \varepsilon_0 \omega \varepsilon''(\omega) \quad (9)$$

and its imaginary part is given by:

$$\sigma''(\omega) = \varepsilon_0 \omega \varepsilon'(\omega) \quad (10)$$

where ε_0 (8.85×10^{-12} Fm^{-1}) is the permittivity of free space and $\omega = 2\pi\nu$ is the angular frequency.

The real and imaginary parts of the σ*(ω) are shown in Figure 6 for neat PVDF and for X= 40%. The conductivity behaviour of the other samples is between that of these samples. For neat PVDF (Figures 6a and 6b), σ´ and σ´´ increase with increasing frequency for all temperatures. This is related to hopping transport of localized charge carriers and is described by the following equation [57]:

$$\sigma'(\omega) \propto \omega^n, n \leq 1 \quad (11)$$

For the whole temperature range, the exponent *n* is the $0.13 < n < 0.9$ range for neat PVDF.

For PVDF/[Emim][TFSI]10% at lower temperatures (below 10 ºC) (see Supplementary Information), frequency dependence of the conductivity follows Eq. (11) with *n* ~0.7 a behaviour reported for charge carrier hopping. For this sample, but at temperatures above 20 ºC, a plateau of σ´, that represents the DC conductivity, followed by an increase of σ' with frequency, due to electrode polarisation, are evident [34]. The plateau is more pronounced for PVDF/[Emim][TFSI] with IL > 10 % (Figure 6c)). On the other hand, the frequency of the maximum in σ" (f_{max}) shown in Figure 6d, which corresponds to the full development of electrode polarization, is better separated from the position f_{on} of the local minimum of σ", indicating the onset of electrode polarization, as indicated in Figure 6d) [34]. The position and intensity of f_{on} and f_{max} increase with the increase of IL content.

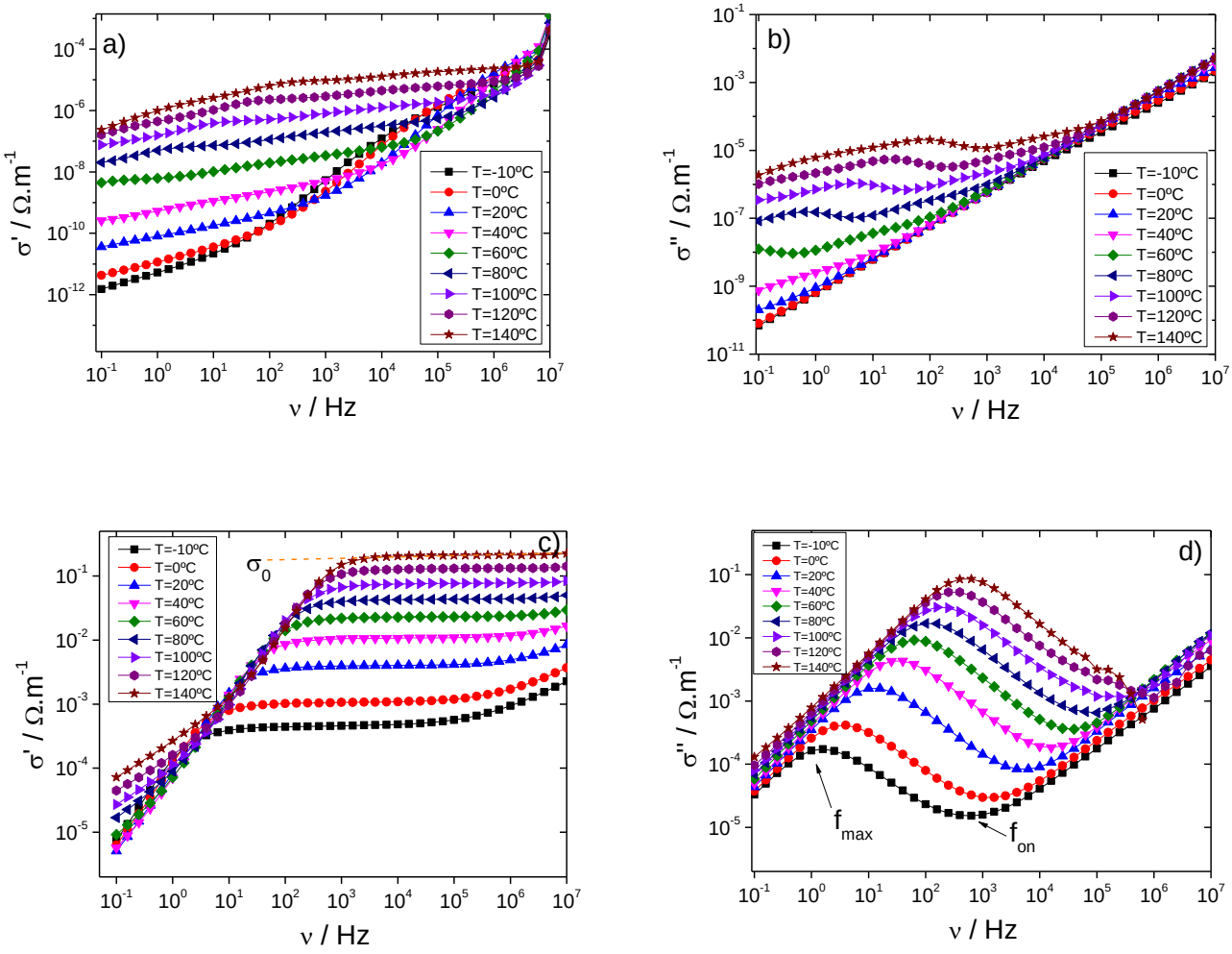

Figure 6 - Frequency dependence of the real and imaginary part of the conductivity (σ*) at different temperatures for neat PVDF (a and b) and PVDF/[Emim][TFSI] 40% (c and d).

Considering that charge transport mechanism at the metal-ion interfaces is described by electrode polarization, Serghei proposed a theoretical approach to calculate the DC conductivity by the following equation into ILs [34]:

$$\sigma_{DC} = 2\pi\varepsilon_0\varepsilon_s \frac{f_{on}^2}{f_{\max}} \qquad (12)$$

where ε_0 is the permittivity of free space and ε_S is the static permittivity of the bulk material measured at $f > f_{on}$.

The DC conductivity obtained from the σ' plateau, illustrated in Figure 6c) for PVDF/[Emim][TFSI]40%, is shown in Figure 7a) for all the PVDF/[Emim][TFSI] samples at different temperatures.

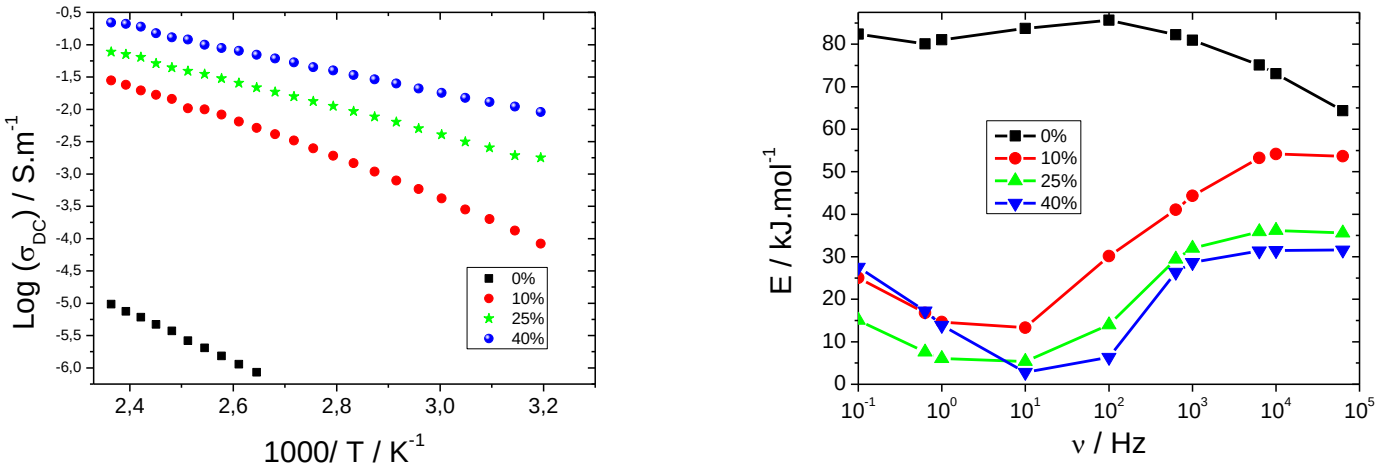

Figure 7 –DC conductivity as a function of temperature a) and evolution of the apparent activation energy obtained after fittings with the Dyre model b) for the PVDF/[Emim][TFSI] samples.

As shown in Figure 7a), DC conductivity increases with the increase of [Emim][TFSI] content because the dissociation and ion transport of the IL results in higher number of charge carriers in the polymer matrix [58].

For the evaluation of the dependence of the AC conductivity with temperature at different frequencies, the Dyre model (random free energy barrier model or symmetric model) was applied [59]:

$$\sigma(T) = Be^{\frac{E}{R.N_A^{-1}.T}} \tag{13}$$

where *B* is a pre-exponential factor identified as the attempt frequency, *E* is the apparent activation energy of the process, T is temperature, R is ideal gas constant and N_A is the Avogadro's number.

The application of the Dyre model was performed considering the real part of the conductivity (σ') between 40 ºC (above T_g) and 140 ºC and in the frequency range between 0.1 Hz and 65 *kHz*. The activation energy, *E*, values calculated are plotted in Figure 7b) as a function of frequency.

In the PVDF sample, the E value decreases with increasing frequency above 10^3 Hz (the change from dc to ac conduction for temperatures above 40 ° C in Fig. 6)). Figure 7b) shows that the addition of the IL leads to the sharp reduction of the activation energy of the process for all frequencies with respect to PVDF, as well as frequency dependence changes. Above 1 Hz, E decreases with the increasing incorporation of [Emim][TFSI] into PVDF matrix. Between 0.1 and 1Hz, the E value decreases with increasing frequency due to the electrode polarization effect into PVDF/[Emim][TFSI] samples. Above of 10^4 Hz for IL=10% and 10^3 for IL=25% and 40%, the E value remains practically constant (Figure 7b). The reason for this behavior is correlated to the plateau zone of Figure 6.

Conclusions

The thermal, mechanical and dielectric properties of PVDF/[Emim][TFSI] blends with different IL contents (10 %≤ IL ≤40%) were characterized to determine the influence of [Emim][TFSI] on the polymer's segmental dynamics and on ionic conductivity. All the techniques showed, not only that IL and PVDF are miscible, but also that the chain segments and the IL are mixed at the nanometer range. This was demonstrated by the shift of the glass transition or the main dielectric or dynamic-mechanical main relaxation towards lower temperatures. Furthermore, the broadening due to composition fluctuations and the fragility of the material decreased due to the participation of the IL in the cooperative rearrangements of the PVDF chain segments. For all the PVDF/[Emim][TFSI] samples, a good agreement between the T_g determined by BDS and DSC was found.

The conductivity formalism revealed that the IL affected the conductivity behavior of the blends from the standpoint of charge motion, ion concentration and electrode polarization effects. For all the doped samples, DC conductivity increased and the apparent activation energy decreased with the increase of IL content. The high DC conductivity value of the [Emim][TFSI]-doped samples in comparison to neat PVDF is due to the ionic dissociation and ion transport of the IL resulting in a higher carrier numbers in the polymer matrix.

Acknowledgements

This work was supported by the Portuguese Foundation for Science and Technology (FCT) in the framework of the Strategic Funding UID/FIS/04650/2013. The authors thank

FEDER funds through the COMPETE 2020 Programme and National Funds through FCT under the projects PTDC/CTM-ENE/5387/2014, PTDC/EEI-SII/5582/2014 and UID/CTM/50025/2013 and Grants SFRH/BPD/121526/2016 (D.M.C.), SFRH/BPD/112547/2015 (C.M.C.). Financial support from the Spanish Ministry of Economy and Competitiveness (MINECO) through the project MAT2016-76039-C4-3-R (AEI/FEDER, UE) (including the FEDER financial support) and from the Basque Government Industry Department under the ELKARTEK Program is also acknowledged. CIBER-BBN is an initiative funded by the VI National R&D&I Plan 2008–2011, Iniciativa Ingenio 2010, Consolider Program. CIBER Actions are financed by the Instituto de Salud Carlos III with assistance from the European Regional Development Fund.

References

[1] M.M. Thackeray, C. Wolverton, E.D. Isaacs, Energy & Environmental Science, 5 (2012) 7854-7863.
[2] G. Majeau-Bettez, T.R. Hawkins, A.H. Strømman, Environmental Science & Technology, 45 (2011) 4548-4554.
[3] B. Nykvist, M. Nilsson, Nature Clim. Change, 5 (2015) 329-332.
[4] A. Arya, A.L. Sharma, Ionics, 23 (2017) 497-540.
[5] P.V. Wright, Electrochimica Acta, 43 (1998) 1137-1143.
[6] F.M. Gray, R.S.o. Chemistry, Polymer electrolytes, Royal Society of Chemistry, 1997.
[7] M. Popall, M. Andrei, J. Kappel, J. Kron, K. Olma, B. Olsowski, Electrochimica Acta, 43 (1998) 1155-1161.
[8] V. Di Noto, S. Lavina, G.A. Giffin, E. Negro, B. Scrosati, Electrochimica Acta, 57 (2011) 4-13.
[9] K. Murata, Electrochimica Acta, 40 (1995) 2177-2184.
[10] C.M. Costa, M.M. Silva, S. Lanceros-Mendez, RSC Advances, 3 (2013) 11404-11417.
[11] H.S. Nalwa, Ferroelectric Polymers: Chemistry, Physics, and Applications, M. Dekker, Incorporated, 1995.
[12] L. Rasmussen, Electroactivity in Polymeric Materials, Springer, 2012.
[13] X. Xue, S. Wang, W. Guo, Y. Zhang, Z.L. Wang, Nano Letters, 12 (2012) 5048-5054.
[14] Z. Wang, ACS Applied Materials & Interfaces, 9 (2017) 15893-15897.
[15] Y.-S. Ye, J. Rick, B.-J. Hwang, Journal of Materials Chemistry A, 1 (2013) 2719-2743.
[16] M.J. Park, I. Choi, J. Hong, O. Kim, Journal of Applied Polymer Science, 129 (2013) 2363-2376.
[17] K.N. Marsh, J.A. Boxall, R. Lichtenthaler, Fluid Phase Equilibria, 219 (2004) 93-98.
[18] H. Niedermeyer, J.P. Hallett, I.J. Villar-Garcia, P.A. Hunt, T. Welton, Chemical Society Reviews, 41 (2012) 7780-7802.
[19] A. Lewandowski, A. Świderska-Mocek, Journal of Power Sources, 194 (2009) 601-609.
[20] C. Xing, Y. Wang, C. Zhang, L. Li, Y. Li, J. Li, Industrial & Engineering Chemistry Research, 54 (2015) 9351-9359.
[21] C. Xing, J. You, Y. Li, J. Li, The Journal of Physical Chemistry C, 119 (2015) 21155-21164.
[22] J. Guan, C. Xing, Y. Wang, Y. Li, J. Li, Composites Science and Technology, 138 (2017) 98-105.
[23] C. Xing, J. Li, C. Yang, Y. Li, Macromolecular Rapid Communications, 37 (2016) 1559-1565.
[24] C. Xing, Y. Wang, X. Huang, Y. Li, J. Li, Macromolecules, 49 (2016) 1026-1035.
[25] C. Xing, M. Zhao, L. Zhao, J. You, X. Cao, Y. Li, Polymer Chemistry, 4 (2013) 5726-5734.
[26] J.C. Dias, M.S. Martins, S. Ribeiro, M.M. Silva, J.M.S.S. Esperança, C. Ribeiro, G. Botelho, C.M. Costa, S. Lanceros-Mendez, Journal of Materials Science, 51 (2016) 9490-9503.
[27] J.C. Dias, A.C. Lopes, B. Magalhães, G. Botelho, M.M. Silva, J.M.S.S. Esperança, S. Lanceros-Mendez, Polymer Testing, 48 (2015) 199-205.
[28] J.R. Sangoro, F. Kremer, Accounts of Chemical Research, 45 (2012) 525-532.
[29] Y. Jiang, H. Nadolny, S. Kashammer, S. Weibels, W. Schroer, H. Weingartner, Faraday Discussions, 154 (2012) 391-407.
[30] S. Agrawal, M. Singh, M. Tripathi, M. Dwivedi, K. Pandey, Journal of Materials Science, 44 (2009) 6060-6068.
[31] S. Havriliak, S.J. Havriliak, Dielectric and Mechanical Relaxation in Materials: Analysis, Interpretation, and Application to Polymers, Hanser Publishers, 1997.
[32] F. Kremer, A. Schönhals, Broadband Dielectric Spectroscopy, Springer, 2003.
[33] K. Nakamura, T. Saiwaki, K. Fukao, Macromolecules, 43 (2010) 6092-6098.
[34] A. Serghei, M. Tress, J.R. Sangoro, F. Kremer, Physical Review B, 80 (2009) 184301.
[35] D. Fragiadakis, S. Dou, R.H. Colby, J. Runt, Macromolecules, 41 (2008) 5723-5728.
[36] P. Frübing, F. Wang, T.-F. Kühle, R. Gerhard, Applied Physics A, 122 (2016) 79.
[37] P. Xu, W. Fu, X. Luo, Y. Ding, Materials Letters, 206 (2017) 60-63.

[38] H. Matsumoto, Recent Advances in Ionic Liquids for Lithium Secondary Batteries, in: T.R. Jow, K. Xu, O. Borodin, M. Ue (Eds.) Electrolytes for Lithium and Lithium-Ion Batteries, Springer New York, New York, NY, 2014, pp. 209-225.
[39] C.M. Costa, H.M. Rodrigues, A. Gören, A.V. Machado, M.M. Silva, S. Lanceros-Méndez, ChemistrySelect, 2 (2017) 5394-5402.
[40] B.-E. El Mohajir, N. Heymans, Polymer, 42 (2001) 5661-5667.
[41] Y.U. Paulechka, A.V. Blokhin, G.J. Kabo, A.A. Strechan, The Journal of Chemical Thermodynamics, 39 (2007) 866-877.
[42] M.P. Silva, C.M. Costa, V. Sencadas, A.J. Paleo, S. Lanceros-Méndez, Journal of Polymer Research, 18 (2011) 1451-1457.
[43] R. Mejri, J.C. Dias, S.B. Hentati, M.S. Martins, C.M. Costa, S. Lanceros-Mendez, Journal of Non-Crystalline Solids, 453 (2016) 8-15.
[44] R. Leones, C.M. Costa, A.V. Machado, J.M.S.S. Esperança, M.M. Silva, S. Lanceros-Méndez, Electroanalysis, 27 (2015) 457-464.
[45] V. Sencadas, S. Lanceros-Méndez, R. Sabater i Serra, A. Andrio Balado, J.L. Gómez Ribelles, The European Physical Journal E, 35 (2012) 41.
[46] F. Frenzel, R. Guterman, A.M. Anton, J. Yuan, F. Kremer, Macromolecules, 50 (2017) 4022-4029.
[47] T. Dam, S.S. Jena, D.K. Pradhan, Physical Chemistry Chemical Physics, 18 (2016) 19955-19965.
[48] R. Sabater i Serra, J.L. Escobar Ivirico, F. Romero Colomer, A. Andrio Balado, J.L. Gómez Ribelles, Journal of Non-Crystalline Solids, 404 (2014) 109-115.
[49] R. Tao, S.L. Simon, The Journal of Physical Chemistry B, 119 (2015) 11953-11959.
[50] S. Firmino Mendes, C.M. Costa, V. Sencadas, J. Serrado Nunes, P. Costa, R. Gregorio, S. Lanceros-Méndez, Applied Physics A, 96 (2009) 899-908.
[51] G. Adam, J.H. Gibbs, The Journal of Chemical Physics, 43 (1965) 139-146.
[52] E. Donth, Journal of Polymer Science Part B: Polymer Physics, 34 (1996) 2881-2892.
[53] J.L. Gómez Ribelles, A. Vidaurre Garayo, J.M.G. Cowie, R. Ferguson, S. Harris, I.J. McEwen, Polymer, 40 (1999) 183-192.
[54] E. Donth, Journal of Non-Crystalline Solids, 53 (1982) 325-330.
[55] M.T. Viciosa, G. Santos, A. Costa, F. Danede, L.C. Branco, N. Jordao, N.T. Correia, M. Dionisio, Physical Chemistry Chemical Physics, 17 (2015) 24108-24120.
[56] A. Vassilikou-Dova, I.M. Kalogeras, Dielectric Analysis (DEA), in: Thermal Analysis of Polymers, John Wiley & Sons, Inc., 2008, pp. 497-613.
[57] A.K. Jonscher, Nature, 267 (1977) 673-679.
[58] R. Leones, C.M. Costa, A.V. Machado, J.M.S.S. Esperança, M.M. Silva, S. Lanceros-Méndez, Solid State Ionics, 253 (2013) 143-150.
[59] J.C. Dyre, Journal of Applied Physics, 64 (1988) 2456-2468.